Interplay of strongly correlated electrons and localized Ising moments in one dimension

Chisa Hotta
Department of Physics, Faculty of Science, Kyoto Sangyo University, Kyoto 603-8555, Japan
(Received 2 December 2009; revised manuscript received 15 March 2010; published 4 June 2010)

We study ground-state properties of a one-dimensional quarter-filled strongly correlated electronic chain coupled to an antiferromagnetic Ising chain by the density-matrix renormalization-group method. We focus on the case where large Coulomb interactions localize the charges on every other site. Both the electronic spins and the Ising moments interact antiferromagnetically within each chain. Since the number of electrons is half as that of Ising moments, the two intrachain Néel orders are incompatible and compete with each other. When the Ising chain is ordered (gapped), the electrons are magnetically frustrated, which is reflected in the nearly degenerate energy levels with different magnetization. The resultant magnetoelectric effect is elucidated as a suppression of a charge gap by the magnetic field.

DOI: 10.1103/PhysRevB.81.245104 PACS number(s): 71.10.Fd, 71.20.Rv, 71.30.+h, 75.50.Dd

I. INTRODUCTION

Physical properties of electrons coupled to localized spins have long been studied in various systems, from Kondo chains in heavy-fermionic systems,[1] double-exchange systems (DEX) in manganites[2] to π-d systems of molecular solids.[3–6] It is worth noting that negative giant magnetoresistance (MR) effect in DEX system provided a mechanism to tune the electronic degrees of freedom by the magnetic field.[2,7] The author and the co-workers tried to figure out another possible mechanism of negative MR by considering a Kondo chain including Coulomb-interaction terms, which we call an extended Kondo lattice model (EKLM).[8] The EKLM was studied with in mind the giant negative MR found in a one-dimensional (1D) organic solid called phthalocyanine salt, TPP$[Fe(Pc)(CN)_2]_2$.[9] The phthalocyanine salt is a quarter-filled π-electronic system which includes a localized Fe d spin on the same TPP molecule.[10] The π electrons have charge order and it is stabilized by the π-d interaction, which is successfully explained by EKLM.[8] However, the EKLM turned out to be different from the experimental situation mainly in two points; the localized moments of TPP$[Fe(Pc)(CN)_2]_2$ have highly anisotropic g factors,[11] and between them, there exists direct interactions. However, in the EKLM the localized spins have SU(2) symmetry and do not have the direct interaction with each other. Therefore we revisit this problem by taking into account the above experimental factors.

The present paper deals with electronic and Ising chains which are interacting ferromagnetically. We focus on the strong-coupling case where the electrons are localized (insulator). Then the system is essentially regarded as double spin chains which have different periodicity of antiferromagnetic intrachain correlation. These correlations compete through the interchain interactions, and when Ising moments are Néel ordered, the electrons become "magnetically frustrated." The paper is organized as follows: Sec. II explains the model and details of the numerical analyses and Sec. III shows the ground-state phase diagram. Section IV is devoted to the clarification of the magnetic properties of the electrons, and finally the external magnetic field is introduced in Sec. V. It turns out that the "magnetic frustration" leads to a nontrivial magnetoelectric effect.

II. MODELS AND METHODS

We consider 1D Ising spin chain and electronic chain which are interacting by the Hund's coupling $-J<0$ at each lattice site. Within the chain, the Ising moments interact antiferromagnetically by $J'>0$, while the electrons have strong on-site and intersite Coulomb interactions, U and V, respectively. The Hamiltonian reads

$$\mathcal{H} = \mathcal{H}_{\rm hubb} + \mathcal{H}_{\rm Ising} + \mathcal{H}_J,$$

$$\mathcal{H}_{\rm hubb} = -\sum_{\langle ij\rangle\sigma} (tc^{\dagger}_{i\sigma}c_{j\sigma} + {\rm H.c.}) + \sum_{\langle ij\rangle} Vn_in_j + \sum_j Un_{j\uparrow}n_{j\downarrow},$$

$$\mathcal{H}_{\rm Ising} = \sum_{\langle ij\rangle} J' S^z_i S^z_j,$$

$$\mathcal{H}_J = -\sum_j JS^z_j s^z_j. \quad (1)$$

Here, the operators $c_{j\sigma}$, n_j, and s^z_j denote the annihilation, the number, and the z component of the spin at jth site for electrons, respectively. We define the magnetization of electrons as $M_{\rm el}=\Sigma_j s^z_j$, and the magnetic density as $m_{\rm el}=M_{\rm el}/N$, where N is the system size. The z component of the localized Ising moment is represented by $S^z_j=\pm 1/2$ and $\langle ij\rangle$ denotes indices of nearest-neighbor pair sites. We focus on the case of quarter-filling of electrons where $4k_F$ instability of the charge degrees of freedom is significantly large.

At $J=0$, each of the decoupled chains has well-defined ground state. The Ising chain is a gapped spin system with Néel order which has $4k_F$ periodicity, $(\uparrow\downarrow\uparrow\downarrow\cdots)$. The Fermi wave number, $k_F=\pi/4$, is defined by the filling factor of electrons. On the other hand, the weak-coupling region of the electronic chain is a Tomonaga-Luttinger liquid (TLL). At quarter-filling, a charge gap opens when the interactions become as large as $U\gtrsim 4t$ and $V\gtrsim 2t$.[12–14] In this ordered (gapped) state, the electrons localize on every other site. The effective antiferromagnetic interaction between the spins of these electrons is given as, $J^0_{\rm eff}=t^4/UV^2$, which leads to $2k_F$-spin-density-wave (SDW) correlation, $[\downarrow\circ\uparrow\circ\cdots]$. Here, $\uparrow$ and $\downarrow$ correspond to up and down spins, respectively, and $\circ$ the absence of charge. Once J is switched on, $(\uparrow\downarrow\uparrow\downarrow\cdots)$ and

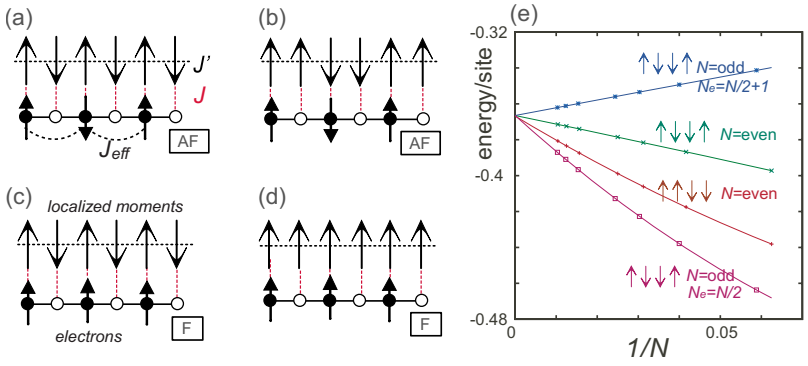

FIG. 1. (Color online) (a)–(d) Representative configurations of localized moments and electrons in the strong-coupling region. (e) Energy per site as a function of $1/N$ at $U/t=8$, $V/t=4$, and $J/t=1$ (charge-ordered state). System-size scaling is given for four different series; odd N with $N_e=N/2$, $N_e=N/2+1$, and even N with $N_e=N/2$ for either $(\uparrow\downarrow\downarrow\uparrow)$- and $(\uparrow\uparrow\downarrow\downarrow)$-Ising spin configurations.

$[\downarrow\circ\uparrow\circ\cdots]$ along the Ising and electronic chains become incompatible. Namely, J favors electronic spins to follow the Néel order of Ising moments and to align ferromagnetically as $[\downarrow\circ\downarrow\circ\cdots]$. Therefore, the competition of J_{eff} with J' and J arises. Such situation is given schematically in Fig. 1(a).

Another reference system is the EKLM in Ref. 8. This model is realized if we replace the interaction of Eq. (1) between electrons and localized spins by that of the SU(2) symmetry, and take $J'=0$. The role of the quantum fluctuation of the localized spins shall be discussed shortly by comparing these two models.

Eigenwave functions of Eq. (1) are a direct product of Ising spin and electronic wave functions. In general, ground state is a superposition of such several different direct products. However, Hamiltonian of Eq. (1) does not mix different Ising spin configurations. Therefore, instead of directly calculating Eq. (1), we can consider the extended Hubbard chain in the presence of periodic field, described by another Hamiltonian

$$\mathcal{H}_{\text{el}} = \mathcal{H}_{\text{hubb}} - \sum_j W_j s_j^z. \tag{2}$$

Here, $W_j=J\langle S_j^z\rangle$ is the on-site "magnetic field" created by the localized Ising moments. The energies of Eq. (1) under all the possible Ising spin configurations are separately obtained as sums of $E_{\text{Ising}}=\langle\mathcal{H}_{\text{Ising}}\rangle$ and $E_{\text{el}}=\langle\mathcal{H}_{\text{el}}\rangle$ from Eq. (2). Then, the lowest energy state among them gives the ground state. We usually do not have superposition of different Ising configurations, except when different configurations give exactly the same energy (which only occurs by accident at finite-system-size calculation).

As a ground-state solver, we use the density-matrix renormalization-group analysis (DMRG).[15] If DMRG is straightforwardly applied to Eq. (1), one finds difficulty in optimizing the Ising configurations. This is because quantum fluctuation which works to improve the selection of the basis in the local update processes is present only in the electron-hopping term. Thus, by calculating Eq. (2) instead of Eq. (1), we can avoid solutions with local-energy minimum which are not the true ground state. Our calculations are developed as follows; (i) assume several different configurations of Ising moments, (ii) calculate $\mathcal{H}_{\text{el}}$ in DMRG under the potentials from each of these configurations at several system size N, and obtain the energy per site in the bulk limit by the finite-size-scaling analysis, and (iii) add to $\langle\mathcal{H}_{\text{el}}\rangle$ the interaction energy of Ising moments, $E_{\text{Ising}}\equiv\langle\mathcal{H}_{\text{Ising}}\rangle$, and get the lowest energy state as a function of J'. Regarding the Ising spin configuration in (i), we consider up to 16-fold periodicity, and it turns out that the states which have twofold or fourfold periodicity give the lowest energies [see Fig. 1(a)]. We thus focus on $(\uparrow\uparrow\downarrow\downarrow)$, $(\uparrow\downarrow\uparrow\downarrow)$, $(\uparrow\uparrow\uparrow\downarrow)$, and $(\uparrow\uparrow\uparrow\uparrow)$ configurations.

Figures 1(a)–1(d) show the representative configurations of Ising moments combined with the unpolarized antiferromagnetic (denoted as AF, $m_{\text{el}}=0$) and fully polarized ferromagnetic (denoted as F, $m_{\text{el}}=0.25\equiv m_{\text{tot}}$) electronic states. In the ground-state phase diagrams of Sec. III we consider only the AF- and F-electronic states, which allows for the systematic finite-size scaling in (ii). We confirmed in advance that the states with ferrimagnetic Ising moments, e.g., $(\uparrow\uparrow\uparrow\downarrow)$, are not ground states for the range of parameters considered. In Sec. V, we also include the Ising configurations up to 32-fold periodicity and calculate the m_{el} dependence by fixing N, in order to examine the effect of magnetic field.

In finite systems with open boundary condition, charges have the largest density at both edge sites. When charges are ordered, they tend to localize on every other site, starting from both ends. A calculation on even-N chain yields a kink structure at the system center, e.g., for $N=8$ we find $(\bullet\circ\bullet\circ\circ\bullet\circ\bullet)$, where $\bullet$ and $\circ$ are the charge-rich and charge-poor sites, respectively. In such a case, the amplitude of the charge density is gradually suppressed toward the center site. If we calculate the odd-N system, this kink disappears, and while the electron number deviates by one from that of the quarter-filling,[16] it is negligible in the bulk limit as $(N_e\pm 1)/N=N_e/N$ at $N\to\infty$. The results of the finite-size scaling of $\mathcal{H}_{\text{el}}$ up to $N=97$ with both odd and even N are presented in Fig. 1(e). The calculation is given in the charge-ordered state for $(\uparrow\downarrow\downarrow\uparrow)$ and $(\uparrow\uparrow\downarrow\downarrow)$ configurations which are equivalent in the bulk limit, and at $N\to\infty$ the energy per site of the four cases in the figure coincides within $<10^{-5}t$. Therefore, energy in the bulk limit is safely obtained.

The $(\uparrow\uparrow\downarrow\downarrow)$ phase shall be regarded as paramagnetic (it actually corresponds to the paramagnetic phase of the Kondo lattice model), since $(\uparrow\downarrow\downarrow\uparrow)$, $(\uparrow\uparrow\downarrow\downarrow)$, and also their mixture dominate the quasidegenerate lowest energy levels at finite system size. These states have intrinsically the same nature and are represented by the $(\uparrow\uparrow\downarrow\downarrow)$ state. In fact, the Ising spin is gapless (or nearly gapless) in this phase (see Secs. IV and V).

By introducing finite J' in (iii), the energy density of $(\uparrow\downarrow\uparrow\downarrow)$ and $(\uparrow\uparrow\uparrow\uparrow)$ states shifts by $-J'/4$ and $J'/4$, respectively, whereas that of the $(\uparrow\uparrow\downarrow\downarrow)$ state does not change. The

lowest energy state among the calculated candidates is thus obtained as functions of U, V, J, and J' at fixed $t=1$.

III. PHASE DIAGRAM

A. Comparison of the ground state of the Ising and SU(2) localized moments at $J'=0$

We first present in Fig. 3(a) the phase diagram at $J'=0$, i.e., when the direct interaction between Ising moments is absent. This diagram is to be compared with the case of EKLM which has the SU(2)-localized moments.[8] At small J, the $(\uparrow\uparrow\downarrow\downarrow)$-Ising moments couple with the AF-electronic state which has $2k_F$-SDW correlation, which undergoes a phase transition into the $(\uparrow\uparrow\uparrow\uparrow)$-Ising moments with fully polarized electrons. This situation has good correspondence with the EKLM; the present $(\uparrow\uparrow\downarrow\downarrow)$ and $(\uparrow\uparrow\uparrow\uparrow)$ states are interpreted as paramagnetic and ferromagnetic states in EKLM, respectively. In the Ising case, the phase boundary shifts to about four times larger value from the SU(2) one. In order to understand this, let us consider the noninteraction case, $U=V=0$. In the EKLM, the ferromagnetic state at large J is characterized by singlet pairs of electrons and localized moments, and the rest of the moments (the electron number is half the number of localized moments) are fully polarized by the hopping of singlets.[17] One can roughly estimate the energy of the paramagnetic and the ferromagnetic states as, $e_{\mathrm{para}}\sim -4\sqrt{2}t+\frac{J}{2}$ and $e_{\mathrm{ferro}}\sim -4t-\frac{J}{4}$, respectively. At $J\sim 2t$, a phase transition takes place. On the other hand, in the Ising case, the band structure is modified under the periodic potential of Ising spins. The energies are given as $e(\uparrow\uparrow\downarrow\downarrow)\sim -\sqrt{\frac{J^2}{16}+2t+\sqrt{\frac{J^2}{4}+2t}}$ and $e(\uparrow\uparrow\uparrow\uparrow)\sim -4t-\frac{J}{4}$. The level crossing occurs at $J/t\sim 6$, which is consistent with the phase diagram. In this way the lack of quantum fluctuation of the Ising moments leads to $e(\uparrow\uparrow\downarrow\downarrow)<e_{\mathrm{para}}$, which originates mainly from the large energy gain of J term in the $(\uparrow\uparrow\downarrow\downarrow)$ state. This is because $(\uparrow\uparrow\downarrow\downarrow)$-AF state is a band insulator at small U and V [while the paramagnetic SU(2) case is a metal]. The energy band splits into four isolated bands under the fourfold periodic potential and the lowest band is completely filled.

Right panel of Fig. 3(a) shows the J/t dependence of energies at $U=V=0$ for all different Ising configurations up to 16-fold periodicity. At $J=0$ all Ising configurations are degenerate, which are separated into several sectors at $J>0$. The $(\uparrow\downarrow\downarrow\uparrow)$ state which corresponds to the $(\uparrow\uparrow\downarrow\downarrow)$ state in the phase diagram has a lowest energy and is well separated from other ferrimagnetic or antiferromagnetic state, except at $J/t<0.005$ where a small ferrimagnetic region is found. The energy differences are relatively small at $U=V=J'=0$, and within the present scheme one cannot completely exclude the possible existence of many phases other than $(\uparrow\uparrow\downarrow\downarrow)$ in the bulk limit. Whereas, once U, V, and J' become finite, the energy separations of $(\uparrow\uparrow\downarrow\downarrow)$, $(\uparrow\downarrow\uparrow\downarrow)$, or ferromagnetic Ising states increase due to large commensurability energy gain in the electronic part, and the phase diagram is well defined.

B. Phase diagram of localized Ising moments

In the next step, we include the J' term and find that the ground state undergoes a phase transition into another magnetic state. Figure 3(b) shows the phase diagrams classified by the configuration of localized moments on the plane of J and J' at several fixed values of U and V in unit of t. Interaction energies of the Ising moments for configurations $(\uparrow\downarrow\uparrow\downarrow)$, $(\uparrow\uparrow\downarrow\downarrow)$, and $(\uparrow\uparrow\uparrow\uparrow)$ are $E_{\mathrm{Ising}}/N=-J'/4$, 0, and $J'/4$, respectively. Therefore, by the introduction of J', $(\uparrow\downarrow\uparrow\downarrow)$ state which gains the energy replaces the others. The boundary of $(\uparrow\downarrow\uparrow\downarrow)$ and $(\uparrow\uparrow\downarrow\downarrow)$ phases are approximately given as $J\sim 4J'$, which is understood by the comparison of magnetic energies of $(\uparrow\downarrow\uparrow\downarrow)$-AF and $(\uparrow\uparrow\downarrow\downarrow)$-AF states in Fig. 1(a); the Ising moments have interaction energies, $E_{\mathrm{Ising}}/N=J'/4$ and 0, respectively. As for the J term, we straightforwardly get $E_J/N=0(\uparrow\downarrow\uparrow\downarrow$-AF) and $J/8(\uparrow\uparrow\downarrow\downarrow$-AF). However, as we see in Sec. III [Fig. 3(d) at $m_{\mathrm{el}}=0$], the amplitude of electronic spin moment in $(\uparrow\uparrow\downarrow\downarrow)$ state is $\langle s_z\rangle\sim 0.25$, which is about half the expected value. This is presumably because the electrons are relatively delocalized to the neighboring site (since one of the neighboring sites has the same potential). The resultant E_J/N of $(\uparrow\uparrow\downarrow\downarrow)$ AF is $J/16$, and after the comparison of $E_{\mathrm{Ising}}+E_J$ in both states, the phase boundary falls on $J\simeq 4J'$.

The phase boundaries are influenced by the electronic interactions as well. By comparing the phase diagrams we find that U stabilizes $(\uparrow\uparrow\uparrow\uparrow)$-F state. This is because the exclusion of double occupancy due to U favors magnetism. On the other hand, $(\uparrow\downarrow\uparrow\downarrow)$-F state ($m_{\mathrm{el}}=m_{\mathrm{tot}}=0.25$) is stabilized by both U and V. When the electronic spins are the fully polarized, J works as potentials to pin the electrons on every other sites, which favors charge order. Typical example is $(\uparrow\downarrow\uparrow\downarrow)$ F with large U and V. This fact is also confirmed in the Monte Carlo study at finite temperature as an enhancement of charge-order correlation by J in Eq. (1).[18] Thus U, V, and J cooperatively stabilize charge order, which is consistent with the results of EKLM.[8]

Phases $(\uparrow\downarrow\uparrow\downarrow)$ and $(\uparrow\uparrow\downarrow\downarrow)$ at $U=8$ given in Fig. 2(b) are insulators. We confirmed this by the finite-size scaling analysis on the charge gap for several choices of parameters. The region of $U/t\gtrsim 4$ and $V/t\gtrsim 2$ is an insulator at $J=0$.[12] The introduction of $J\neq 0$ stabilizes the insulating phase for both cases, $(\uparrow\downarrow\uparrow\downarrow)$ and $(\uparrow\uparrow\downarrow\downarrow)$. In the next section, we discuss the magnetic properties of these insulating phases.

IV. MAGNETIC PROPERTIES

A. Competing magnetic orders

The ground-state phase diagrams are basically dominated by $(\uparrow\downarrow\uparrow\downarrow)$ and $(\uparrow\uparrow\downarrow\downarrow)$ phases. So far, in these phases the spin-unpolarized $m_{\mathrm{el}}=0$ (AF) and fully spin-polarized $m_{\mathrm{el}}=m_{\mathrm{tot}}$ (F) electronic states are examined. In the next step, we calculate m_{el} dependence of energy by DMRG. Here, we focus on the large U and V regions where the system is a charge-ordered insulator. The nontrivial competition among J, J', and J_{eff} discussed in Sec. II shall be examined explicitly, where J_{eff} is the effective interaction between electronic spins localized on every other site. Figures 3(a) and 3(b) show the electronic energy per site, $E(m_{\mathrm{el}})/N$ under the above mentioned two different configurations for several choices of J at $N=64$, $U/t=8$, and $V/t=4$. In the $(\uparrow\downarrow\uparrow\downarrow)$ state, the functional form of $E(m_{\mathrm{el}})$ is flattened as J increases.

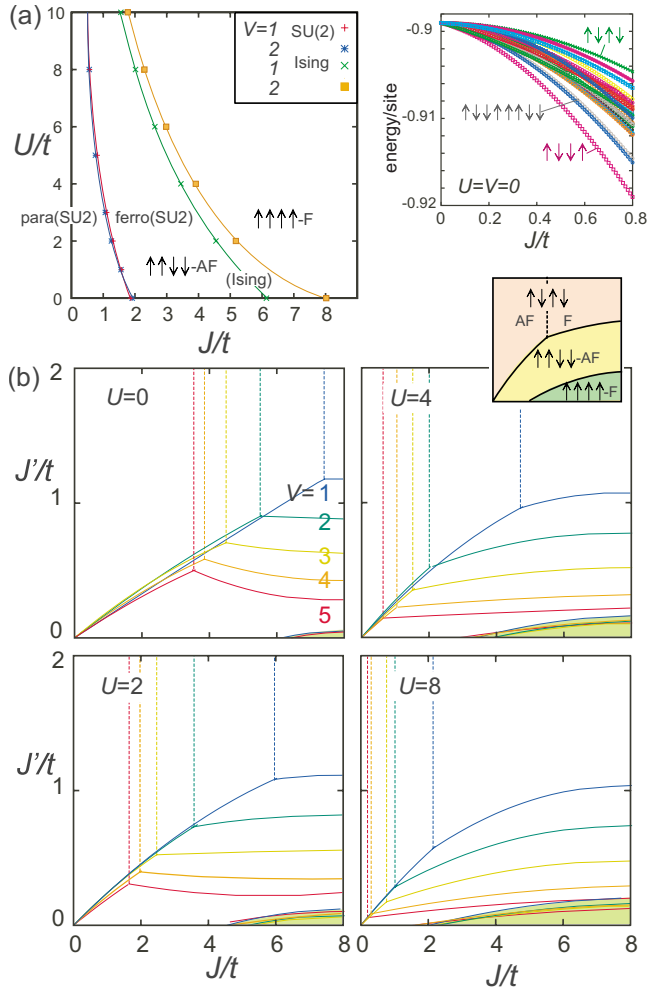

FIG. 2. (Color online) (a) Phase diagram at $J'=0$ on the plane of U/t and J/t for $V/t=1$, 2. Phase boundary of the extended Kondo lattice model in Ref. 8 is plotted together for comparison. Right panel shows the electronic energy per site for all different configurations up to 16-fold periodicity of Ising moments as a function of J/t at $U=V=0$ and at $N=24$. (b) Phase diagrams on the plane of J/t and J'/t for $U/t=0$, 2, 4, 8 and $V/t=1$, 2, 3, 4, 5. The diagrams are separated into four regions, $(\uparrow\uparrow\downarrow\downarrow)$ AF, $(\uparrow\downarrow\uparrow\downarrow)$ AF, $(\uparrow\downarrow\uparrow\downarrow)$ F, and $(\uparrow\uparrow\uparrow\uparrow)$ F, which are shown schematically in Figs. 1(a)–1(d). Here, AF and F denote the unpolarized and fully polarized electronic spins, $m_{\rm el}=0$ and 0.25, respectively.

Contrastingly, $E(m_{\rm el})$ of the $(\uparrow\uparrow\downarrow\downarrow)$ state becomes a more rapid increasing function at larger J.

The charge and electronic spin densities at $m_{\rm el}=0$ and $m_{\rm tot}$ under $(\uparrow\downarrow\uparrow\downarrow)$ and $(\uparrow\uparrow\downarrow\downarrow)$ configurations are given in Figs. 3(c) and 3(d). The spin densities differ significantly between the two figures; at $m_{\rm el}=0$, $(\uparrow\downarrow\uparrow\downarrow)$ state has small amplitude of $\langle s_z\rangle$ compared to that of $(\uparrow\uparrow\downarrow\downarrow)$. The $4k_F$ periodicity of $(\uparrow\downarrow\uparrow\downarrow)$ has misfit with the $2k_F$ correlation $[\downarrow\circ\uparrow\circ]$ along the electronic chain. Therefore, $\langle s_z\rangle$ is rather suppressed due to the magnetic frustration between two different chains. In contrast, in the $(\uparrow\uparrow\downarrow\downarrow)$ state the $2k_F$-antiferromagnetic correlations along both chains cooperate and enhance the amplitude of the spin moments. When the electrons become fully polarized at $m_{\rm el}=m_{\rm tot}$, the magnetic frustration in the former $(\uparrow\downarrow\uparrow\downarrow)$ state is resolved so that the difference between the two configurations becomes almost negligible.

The spin gap is shown in Figs. 3(e) and 3(f) as a function of J/t at $U/t=8$ and $V/t=4$, which is obtained after the extrapolation to the bulk limit. Both cases starts from a gapless state at $J=0$. Under $(\uparrow\downarrow\uparrow\downarrow)$ configuration, a small gap opens first and then closes again already at extremely small J. As for the $(\uparrow\uparrow\downarrow\downarrow)$ case the spin gap continues to increase as a function of J. These results are consistent with the findings in Figs. 3(a) and 3(b).

As we discussed in Sec. III, charge order is stabilized by the polarization of electronic spins in both $(\uparrow\downarrow\uparrow\downarrow)$ and $(\uparrow\uparrow\downarrow\downarrow)$ cases. Actually, the amplitude of $\langle n_i\rangle$ increases with increasing $m_{\rm el}$. It is interesting to find that $\langle n_i\rangle$ does not seem to differ between $(\uparrow\downarrow\uparrow\downarrow)$ and $(\uparrow\uparrow\downarrow\downarrow)$ cases even at small $m_{\rm el}$ where the magnetic properties of the two significantly differ. Namely, at quarter-filling the charge degrees of freedom is approximately decoupled from the spin degrees of freedom. This does not hold off quarter-filling which we discuss in Sec. V.

Spin gap on the Ising chain is defined by $\Delta_{\rm Ising}=E_{\rm el}(S_z=1,\ s_z=0)-E_{\rm el}(S_z=0,\ s_z=0)+E_{\rm Ising}(S_z=1)-E_{\rm Ising}(S_z=0)$, where the first two terms are the energies of electronic chain under different Ising configurations, and S_z/s_z are the total z component of Ising/electronic spins. At $J=0$, the gap is that of the isolated Ising chain, and $(\uparrow\downarrow\uparrow\downarrow)$ and $(\uparrow\uparrow\downarrow\downarrow)$ states have $\Delta_{\rm Ising}=J'$ and 0, respectively. At $J>0$ the gap has contributions from the electronic energies, and we find that $(\uparrow\downarrow\uparrow\downarrow)$ and $(\uparrow\uparrow\downarrow\downarrow)$ states remain basically gapped and gapless, respectively. The evaluation of Ising gap after the size scaling yields $\Delta_{\rm Ising}\gtrsim\mathcal{O}(J)+J'$ for $(\uparrow\downarrow\uparrow\downarrow)$ state and $\Delta_{\rm Ising}<0.05t$ (even if gapped, it remains one orders of magnitude small compared to J) for $(\uparrow\uparrow\downarrow\downarrow)$ state, which are consistent with the magnetic phase diagram in Sec. V.

B. Strong-coupling approach

In order to understand the nature of such spin degrees of freedom in the insulating states we derive the effective Hamiltonian of the electronic spins by the perturbative approach. We start from the strong-coupling limit, $U/t, V/t, U/J, V/J\to\infty$, where the charges localize on every other site as shown in Figs. 4(a) and 4(b). At the first-order perturbative level of J, the $\mathcal{H}_{\rm Ising}$ term in Eq. (1) works as an effective internal magnetic field, $H_{\rm eff}$, on these electronic spins. Then electronic system is described by a noninteracting SU(2) spin chain under the (internal) magnetic field. Spin-exchange interactions within the electronic chain appear in the perturbation processes at fourth order of t. Figure 4(c) shows processes which mix the adjacent spins (by two lattice spacing). Then, $\mathcal{H}_{\rm el}$ in Eq. (2) is transformed to the effective Hamiltonian given as

$$\mathcal{H}_{\rm eff}=\sum_{j=2l\ (l=\text{integer})}[J^z_{\rm eff}s^z_js^z_{j+2}+J^\perp_{\rm eff}(s^x_js^x_{j+2}+s^y_js^y_{j+2})-s^z_jH_{\rm eff}(l)]. \tag{3}$$

Here, $H_{\rm eff}$ is a l-dependent internal magnetic field from the localized Ising moments. For $(\uparrow\downarrow\uparrow\downarrow)$ state we have

$$J^z_{\rm eff}=\frac{2t^4}{U}\left(\frac{1}{(V+J/2)^2}+\frac{1}{(V-J/2)^2}\right),$$

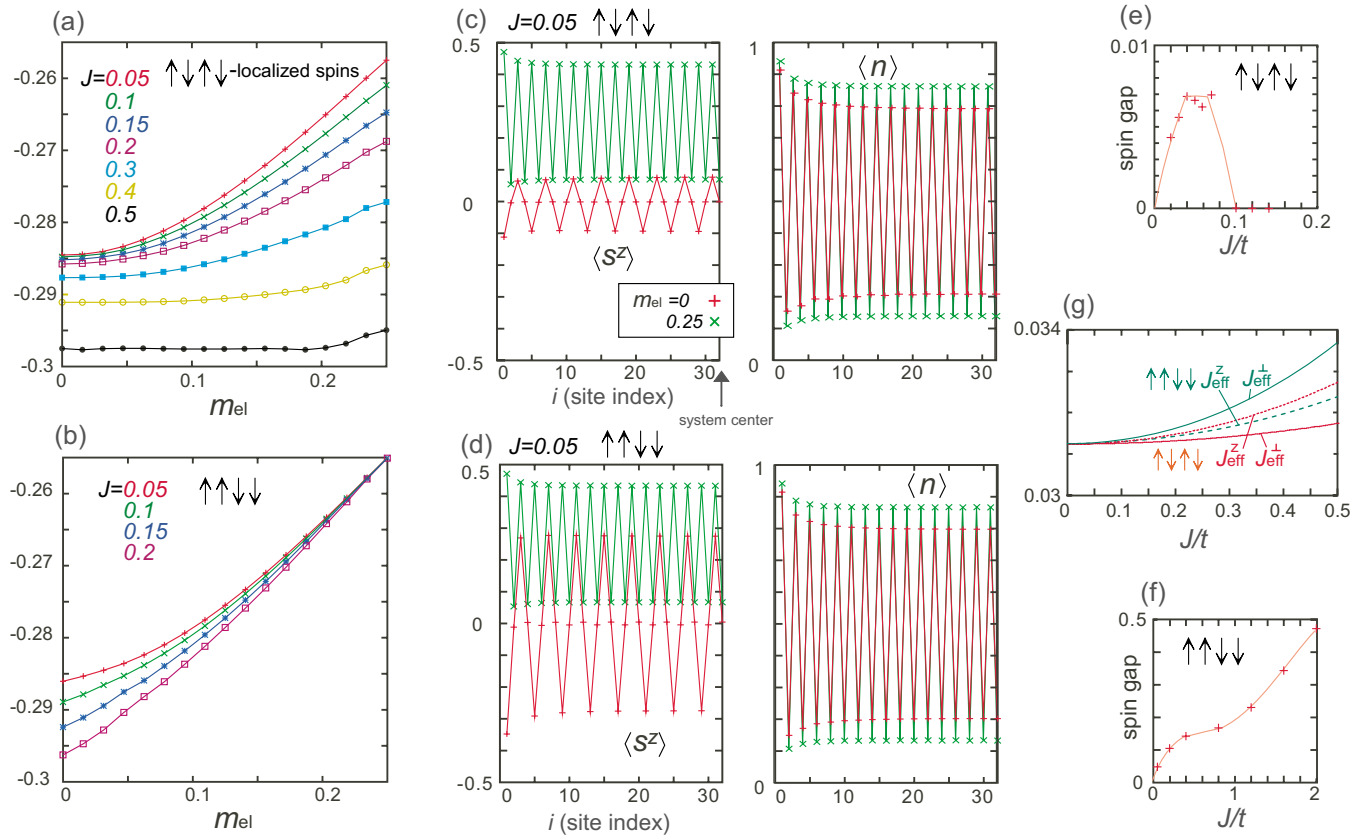

FIG. 3. (Color online) Panels (a) and (b) are the $m_{\rm el}$ dependence of energy per site, $E(m_{\rm el})/N$, at $N=64$ with $(\uparrow\downarrow\uparrow\downarrow)$- and $(\uparrow\uparrow\downarrow\downarrow)$-Ising spin configurations, respectively, at $U/t=8$ and $V/t=4$ for various choices of J/t. Panels (c) and (d) are the local charge and spin densities, $\langle n_i\rangle$ and $\langle s_i^z\rangle$, which correspond to (a) and (b), respectively, at $J/t=0.05$. Panels (e) and (f) are the spin gap in the bulk limit as a function of J/t at $U/t=8$ and $V/t=4$ for $(\uparrow\downarrow\uparrow\downarrow)$ and $(\uparrow\uparrow\downarrow\downarrow)$ cases. Panel (g) gives the effective spin-spin interaction $J_{\rm eff}$ evaluated using Eqs. (4) and (5) as a function of J/t at $U/t=8$ and $V/t=4$.

$$J_{\rm eff}^{\perp}=\frac{4t^4}{U}\frac{1}{V^2-(J/2)^2},$$

$$H_{\rm eff}=\frac{J}{2}, \tag{4}$$

where $J_{\rm eff}^{z}>J_{\rm eff}^{\perp}$. Therefore, the system is *an XXZ-spin system with Ising anisotropy in the uniform magnetic field*. When finite J is introduced the spin gap opens, which, however, is suppressed immediately by the magnetic field when J increases further. We show $J_{\rm eff}$'s as a function of J/t in Fig. 3(g) evaluated from Eq. (4) at $U/t=8$ and $V/t=4$. Actually, the increase in $J_{\rm eff}$ is slower than that of $H_{\rm eff}$. Therefore, even though the anisotropy of interaction, $J_{\rm eff}^{z}/J_{\rm eff}^{\perp}$, increases as a function of J, the uniform magnetic field $H_{\rm eff}$ has larger magnitude and the spin sector is gapless.

On the other hand, the $(\uparrow\uparrow\downarrow\downarrow)$ Ising configuration yields the following effective parameters:

$$J_{\rm eff}^{z}=t^4\left\{\left[\frac{1}{V^2}+\frac{1}{(V+J/2)^2}\right]\frac{1}{U+J/2}\right\}+\left[\frac{1}{V^2}+\frac{1}{(V-J/2)^2}\right]\frac{1}{U-J/2},$$

$$J_{\rm eff}^{\perp}=t^4\left\{\frac{1}{V}\left[\frac{1}{(V+J)(U+J/2)}+\frac{1}{(V-J)(U-J/2)}\right]+\frac{1}{(V+J/2)^2(U+J/2)}+\frac{1}{(V-J/2)^2(U-J/2)}\right\},$$

$$H_{\rm eff}=(-)^l\frac{1}{2}\left\{J+\left[\frac{1}{V^2}+\frac{1}{(V+J/2)^2}\right]\frac{t^4}{U+J/2}-\left[\frac{1}{V^2}+\frac{1}{(V-J/2)^2}\right]\frac{t^4}{U-J/2}\right\}. \tag{5}$$

This time we have $J_{\rm eff}^{z}<J_{\rm eff}^{\perp}$, and the system is interpreted as *an XXZ-spin chain with XY-anisotropy* (TLL) *placed under the staggered magnetic field*. Figure 3(g) shows $J_{\rm eff}$'s as a function of J. Again, the internal field overwhelms the effective spin interactions. The Néel order is stabilized, which has larger spin gap compared to the $(\uparrow\downarrow\uparrow\downarrow)$ state [see Fig. 3(f)]. This is because the antiferromagnetic correlation on two chains cooperate by J. The large $\langle s_z\rangle$ of local moments in the DMRG calculation in Fig. 3(d) actually supports this scenario.

At $J=0$, the effective Hamiltonians, Eqs. (4) and (5) are reduced to the simple Heisenberg spin Hamiltonian without the magnetic field ($H_{\rm eff}=0$), which has a SU(2) spin-spin

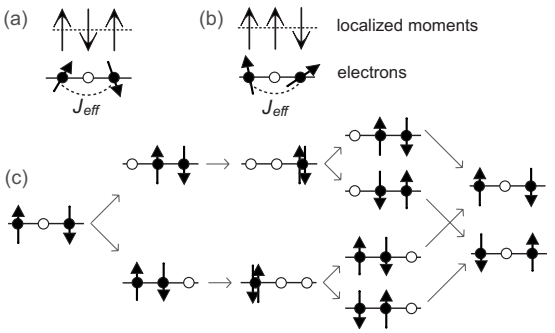

FIG. 4. The representative charge-ordered state at large U/t and V/t for (a)$(\uparrow\downarrow\uparrow\downarrow)$ and (b)$(\uparrow\uparrow\downarrow\downarrow)$ configurations, where the Ising moments work as internal uniform and staggered field to the electronic spins, respectively. Panel (c) is the fourth-order perturbative process by the hopping of electrons. The processes themselves are common between (a) and (b) while the energy of the initial, final, and intermediate states in the processes differ due to different configuration of Ising moments.

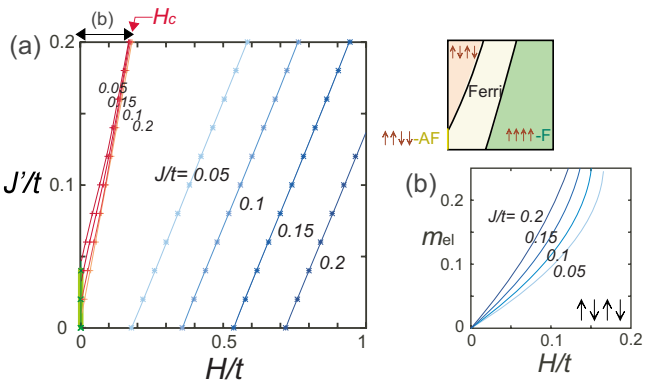

FIG. 5. (Color online) DMRG results analyzed by the combination with the external magnetic field (H) at $U/t=8$, $V/t=4$, and $N=64$. Panel (a) is the phase diagram on the plane of J' and H. Panel (b) gives the magnetization, m_{el}, of the $(\uparrow\downarrow\uparrow\downarrow)$ phase at the small H (the corresponding region is indicated by arrows above the phase diagram).

interaction, $J^{z}_{eff}=J^{\perp}_{eff}=t^4/(UV^2)\equiv J^0_{eff}$, which we mentioned in Sec. II. The SU(2) symmetry of J_{eff} at $J\neq 0$ is thus modified to a Z(2) one by the localized Ising moments.

V. EXTERNAL MAGNETIC FIELD

A. Phase diagram under external field

Finally, we introduce the external magnetic field, H, to the present system. Figure 5(a) shows a phase diagram on the plane of J'/t and H/t for several choices of J at $N=64$. We consider the Ising configuration up to 32-site periodicity, all possible degrees of electronic polarization, m_{el}, and determine the lowest energy state. The phase diagram is classified into four parts; at small J' and $H\sim 0$, the $(\uparrow\uparrow\downarrow\downarrow)$ phase exists, which is immediately replaced by the ferrimagnetic phase at finite H. These ferrimagnetic states are periodic ones, e.g., those with fourfold, $(\uparrow\uparrow\uparrow\downarrow)$, or eightfold periodicity, $(\uparrow\uparrow\uparrow\uparrow\uparrow\uparrow\uparrow\downarrow)$. The magnetic moments on both chains saturates at $H_s\sim 4J+2J'$ [which is the onset of $(\uparrow\uparrow\uparrow\uparrow)$-F state]. At larger J', the $(\uparrow\downarrow\uparrow\downarrow)$ phase extends from $H=0$ toward finite H.

Here, again $(\uparrow\downarrow\uparrow\downarrow)$ and $(\uparrow\uparrow\downarrow\downarrow)$ states significantly differ regarding the instability against the external magnetic field. The former sustains at $0\leq H\leq H_c$, whereas the latter is unstable and disappears at finite H. This is because the Ising chain is gapped in the former and is gapless in the latter. In the former $(\uparrow\downarrow\uparrow\downarrow)$ phase the Ising-Néel order is stable while gapless electronic chain (see Sec. IV) is gradually magnetized with H. One can adopt the magnetization curve in Fig. 5(b) to the $(\uparrow\downarrow\uparrow\downarrow)$ phase in Fig. 5(a) along the H/t axis regardless of the value of J'/t. As we saw in Fig. 3(a) the m_{el} dependence of energy of this charge-ordered state became nearly flat as J increased. Therefore, the Zeeman term of the electronic spins "absolves" the effect of the external magnetic field before the localized spins start to flip at $H=H_c$ [which is a $(\uparrow\downarrow\uparrow\downarrow)$-ferrimagnetic phase boundary in Fig. 5(a)].

B. Charge gap under the external field

We discussed in Sec. IV [Fig. 3(c)] that the degree of charge disproportionation in the $(\uparrow\downarrow\uparrow\downarrow)$-charge-ordered state increases by the polarization of electronic spins. Therefore, the charge gap is also expected to increase with m_{el}. We calculate the energy gap $\Delta_o=E(N_e-1)+E(N_e+1)-2E(N_e)$ as a function of m_{el}. In evaluating Δ_o at (N_e,m_{el}) with $N_e=N/2$, we take either of the magnetic polarization $m_{el}\pm 1$ which gives the lower energy in both the electron-doped (N_e+1) and hole-doped (N_e-1) states. The result as a function of m_{el} is shown in Fig. 6(a) for several choices of J. As expected, the fully polarized state has larger Δ_0 than the unpolarized state. However, at intermediate $0<m_{el}<m_{tot}$ we find significant decrease in Δ_0. The decrease is several orders of magnitude larger compared to the variation in Δ_0 induced by J at $m_{el}=0$ [see the lower panel of Fig. 6(a)]. Since Δ_0 decreases the most significant at $J=0$, it is not attributed to J.

Let us examine the particular m_{el} dependence of Δ_0. Figure 6(b) shows the contributions from interactions and kinetic energies [i.e., U, V, J, and t terms of Eq. (1)] separately as functions of m_{el} denoted as Δ_U, Δ_V, Δ_J, and Δ_t. As $m_{el}[=(N_{e\uparrow}-N_{e\downarrow})/2]$ increases, effect of Pauli's principle becomes pronounced; the number of particles which can have double occupancy decreases, and the kinetic-energy gain becomes small. Thus, the corresponding energies, Δ_U and Δ_t, needed to add one particle (electron or hole) increase and decrease, respectively, by m_{el}. Then, at $m_{el}\sim m_{tot}/2$, Δ_U changes sign from positive to negative, namely, the degree of double occupancy of charges increases by adding particle at $m_{el}<m_{tot}/2$, while it decreases at $m_{el}>m_{tot}/2$. Accordingly, Δ_t changes sign oppositely near this point. From these results, the following two different pictures on the rearrangement of electrons are obtained. At $m_{el}<m_{tot}/2$, the $(N_e\pm 1)$ states become metallic by itinerating more charges than the (N_e) state, where the system can gain kinetic energy $(E_t<0)$ which overwhelms the interaction-energy loss $(\Delta_V,\Delta_U>0)$. On the other hand, at $m_{el}>m_{tot}/2$, the system rearranges the charge distribution in such a way to increase the charge-order amplitude $(\Delta_V,\Delta_U<0)$ by sacrificing the kinetic-energy loss $(\Delta_t>0)$. At $m_{el}\sim m_{tot}/2$, the crossover between these two pictures takes place and $|\Delta_t|$, $|\Delta_U|$, $|\Delta_V|$ takes roughly the minimum. Therefore, at this point, the degree of rearrangement of electrons through $(N_e)\rightarrow(N_e\pm 1)$ is the smallest.

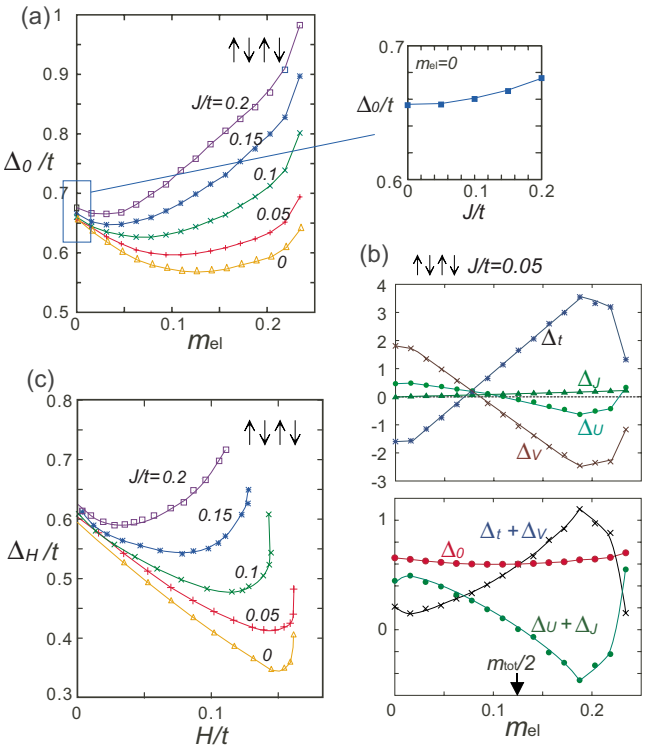

FIG. 6. (Color online) Panels (a) and (c) are "energy gap" in the $(\uparrow\downarrow\uparrow\downarrow)$ state at $H=0$ (Δ_0 without the Zeeman term) and $H\neq 0$ (Δ_H including the Zeeman term) as a function of $m_{\rm el}$ and H, respectively, where (c) corresponds to the charge gap under the magnetic field. The charge gap (Δ_0 at $m_{\rm el}=0$) at $H=0$ as a function of J is shown together. Panel (b) is the decomposition of Δ_o into Δ_U, Δ_V, Δ_t, and Δ_J, which are the contributions from U, V, J, and t terms in Eq. (1). (The upturn/downturn of Δ_V/Δ_t at $m_{\rm el}\gtrsim 0.2$ is related to the significant enhancement of ground-state charge order at $m_{\rm el}\sim m_{\rm tot}$ and is not explained in the main text for simplicity.)

Namely, the ground state is the most close to the metallic excited states and thus the charge gap is minimized. As shown in the lower panel of Fig. 6(b), the intersite contribution, $\Delta_t+\Delta_V$, and the on-site contributions, $\Delta_U+\Delta_J$, are convex downward and upward functions, respectively, and since the former has large amplitude, Δ_0 is convex downward and takes the minimum at $m_{\rm el}\sim m_{\rm tot}/2$.

The convex downward functional form of Δ_0 is the most significant at $J=0$, while its both edges have the comparable values, $\Delta_0(m_{\rm el}=0)\sim\Delta_0(m_{\rm el}=m_{\rm tot})$. When $J>0$, kinetic-energy gain is significantly suppressed at $m_{\rm el}>0$, since the polarized electrons are pinned on every other site by localized moments. Thus, E_t of the (N_e+1) state at $m_{\rm el}>0$ increases with J, particularly at smaller $m_{\rm el}$ which was originally more itinerant. Then, the convex functional form dissolves and Δ_0 is gradually transformed toward a monotonically increasing function of $m_{\rm el}$ with increasing J.

Next, we include the Zeeman term and calculate the charge gap against the external magnetic field, which is denoted as Δ_H. Reflecting the functional form of Δ_0, it appears as a convex-downward function as shown in Fig. 6(c). Here, for the doped cases we again choose either of the $m_{\rm el}\pm 1$ which gives the lower energy including the Zeeman terms. Notice that we neglect the orbital effect under the external field, which we consider to be small in one dimension. Particularly at small J/t, Δ_H continues to decrease significantly toward $H/t\sim 0.1$–0.2. Going back to the phase diagram in Fig. 5(a), we can expect that the upturn of the gap does not appear in overall in the $(\uparrow\downarrow\uparrow\downarrow)$ phase, $H\leq H_c\sim J'\lesssim 0.1$.

In this way, owing to the stable $(\uparrow\downarrow\uparrow\downarrow)$-Ising state, the magnetic field works only on the charge-ordered electronic chain and suppresses the charge gap Δ_H. The corresponding negative magnetoresistance shall be expected which has origin different from the double-exchange systems.

VI. SUMMARY AND DISCUSSIONS

In the present paper, we disclosed the intriguing interplay of magnetic and electric properties of the quarter-filled strongly correlated electronic chain coupled to the Ising moments. Almost regardless of the details of the electronic state, the ground state is in overall classified by the two different configurations of Ising moments, $(\uparrow\uparrow\downarrow\downarrow)$ and $(\uparrow\downarrow\uparrow\downarrow)$ at $J\gtrsim 4J'$ and $J\lesssim 4J'$, respectively. The former is an analog of the paramagnetic state in the Kondo lattice model which has Ruderman-Kittel-Kasuya-Yoshida (RKKY) interaction through J. The latter is stabilized by the direct interaction between Ising moments, J'.

The main focus is an interplay of spin and charge degrees of freedom in the insulating charge-ordered state at large U and V. In the strong-coupling picture, electrons are localized on every other site, whose spins are interacting antiferromagnetically via $J_{\rm eff}$. The Ising moments work as effective internal field $|H_{\rm eff}|\sim J/2$ to these electronic spins. At the same time the Ising moments modify the symmetry of the interaction, $J_{\rm eff}$, from SU(2) at $J=0$ to Z(2). Thus, the electronic spins coupled to $(\uparrow\downarrow\uparrow\downarrow)$ moments behave as an Ising XXZ-spin system under uniform magnetic field, while the ones coupled to $(\uparrow\uparrow\downarrow\downarrow)$ moments as an XY-spin system under staggered magnetic field. The Ising chain is gapped $(\uparrow\downarrow\uparrow\downarrow)$ and gapless $(\uparrow\uparrow\downarrow\downarrow)$, whereas electronic chain is vice versa.

The more intuitive description is given in the following. The period of antiferromagnetic correlation $[\downarrow\circ\uparrow\circ]$ of electronic chain differs by twice from that of Ising chain $(\uparrow\downarrow\uparrow\downarrow)$, while the same as $(\uparrow\uparrow\downarrow\downarrow)$. In the former $(\uparrow\downarrow\uparrow\downarrow)$ case, due to the magnetic misfit (or frustration) of two chains, electronic chain becomes magnetically fragile under the Néel order of Ising moments. The magnetic field gradually magnetizes the electronic chain and suppresses the charge gap, while the Ising-Néel order sustains. Contrastingly, the latter gapless $(\uparrow\uparrow\downarrow\downarrow)$-Ising state is easily destroyed by the external magnetic field.

We conclude that the present two-chain system has a particular competition of J, J', and $J_{\rm eff}$, which allows for the coexistence of completely different magnetic properties between the Ising and electronic chains, namely, either is gapped and the other is gapless. In other words, Néel orders of the two chains are incompatible. When the Ising chain has a Néel order $(\uparrow\downarrow\uparrow\downarrow)$ due to J', the electronic chain is magnetically frustrated and shows nearly degenerate energy structure as a function of $m_{\rm el}$.

The similar picture shall also be found in EKLM. Paramagnetic state of EKLM corresponds to $(\uparrow\uparrow\downarrow\downarrow)$ in the

present study. The $(\uparrow\uparrow\downarrow\downarrow)$ *order* is weakened in EKLM by the quantum fluctuation to the antiferromagnetic *correlation* which cooperates with J_{eff} via RKKY interaction.[17] When J becomes large, the SU(2) spins form singlets with the electrons, which propagate and stabilize ferromagnetism.[17] Therefore, if one includes the direct interaction, J', between SU(2) spins, it favors antiferromagnetism and competes with the J-induced ferromagnetism. Thus, a similar magnetic frustration may appear. However, such physical picture shall be rather blurred by the quantum fluctuation [SU(2)]. The present Ising spin system has a more serious frustration effect, which may lead the electronic system to a sensitive response to the magnetic field. While the DMRG study on the ferromagnetic KLM, a SU(2) version of the present model, is previously carried out, they focus on large $J \gg t$ region[19] in the context of manganites, whose picture regarding the origin of charge order and magnetism are completely different from the one presented here.

Finally, let us examine the relevance of these results with the experiments on the TPP$[M(\mathrm{Pc})(\mathrm{CN})_2]_2$, $M=\mathrm{Fe},\mathrm{Co}$.[10] The Co salt is a pure electronic chain ($J=0$ in the present model), which is a good reference system to analyze the effect of localized moments. Both salts have semiconducting temperature dependence of resistivity. The Fe salt shows a large negative MR which amounts to $\rho(H)/\rho(0) \sim 10^{-2}$, where $\rho(H)$ is the resistivity under the magnetic field H. The experimental findings are summarized as follows. (1) The activation energy derived from resistivity data are $\Delta_a \sim 10^{-3}$ and $\sim 10^{-2}$ eV for Co and Fe salts, respectively.[9] (2) Localized moment has anisotropic g values, $g_\perp \sim 3.6$ and $g_\parallel \sim 0.5-1$ which are roughly perpendicular and parallel to the molecular axis, respectively. This anisotropy is explained in terms of spin-orbit coupling and the resultant magnetic moment is $S=1/2$.[11] (3) Magnetic susceptibility shows a large anisotropy, $\chi_\perp/\chi_\parallel > 5$, and $\chi_\parallel$ gives similar values with the Co one.[9] (4) Residual magnetization is observed at $T < 12$ K, which is attributed to the ferrimagnetism of π electrons by the torque experiment.[20] (5) MR is not scaled by the magnetization and shows large-T dependence.[21] (6) Phase transition is absent (in contrast to DEX), namely, the scenario of the competition of two different orders are not applicable. (7) MR is relevant when Fe ion is partially replaced by Co ion, e.g., even when the degree of replacement is as large as $\mathrm{Fe}_{0.07}\mathrm{Co}_{0.93}$, the MR amounts to $\rho(H)/\rho(0) \sim 0.5$.[22] (8) Magnetization of electrons gradually increases with H and that of the Fe moments starts at $H_c \sim 15$ T.[23] (9) Ground state of the electronic chain is weakly charge ordered which is observed by the nuclear quadrupole resonance study.[21]

The factors (2) and (9) are taken into account in the present model. The parameter values estimated from the extended Hückel calculation, *ab initio* calculation, and by the reflectance spectra give $t \sim 0.1$ eV, $J \sim t/10$, and $J' \sim J/3$, where J and J' are Hund's and exchange coupling constants, respectively. If we put these parameters in the phase diagram of Fig. 2(b), it is located within the $(\uparrow\downarrow\uparrow\downarrow)$ phase. Magnetic properties of electrons behave quite sensitive to U and V; when $U=8$ and $V=4$, the system is in the vicinity of the AF-F phase boundary in Fig. 2(b). Figure 3(a) shows that m_{el} dependence of energy is small. Then, the ferrimagnetism of π electrons is possible, which is consistent with (4). The external field gradually magnetizes the π electrons, and the onset of flipping of localized moments, $H_c \sim 0.01$ T in (8) is consistent with the phase diagram in Fig. 5(a) (at $J'/t \sim 0.1/3$). In this way, we reach the picture that electrons of the phthalocyanine Fe salts show fragile magnetic properties while the Fe moments have the stable antiferromagnetic order due to J' in the ground state. Actually, (4) is well explained as a weak ferrimagnetism of electrons under magnetic frustration.

However, there still remains some issues to be clarified; in our model, the charge gap decreases with H, while it does decrease even at $J=0$. Therefore, J does not seem to favor the suppression of charge order by the magnetic field. The Co salt (corresponding to $J=0$) shows a small but positive MR,[21] which is incompatible with our results. Also the present model which focuses on the particular density of d spins cannot cope with issue (7). Therefore, in order to clarify fully the origin of MR, a more systematic experimental data (regarding the Fe-Co ratio or the effect of the dimensionality of the system) as well as the theoretical calculations directly on the transport properties shall be required.

ACKNOWLEDGMENTS

The author acknowledges N. Hanasaki, M. Takigawa, M. Kimata, and H. Tajima for helpful discussions and comments. This work is supported by Grant-in-Aid for Scientific Research (Grants No. 19740218, No. 21110522, and No. 22014014) from the Ministry of Education, Science, Sports and Culture of Japan.

[1] G. Aeppli and Z. Fisk, Comments Condens. Matter Phys. **16**, 155 (1992).
[2] A. Moreo, S. Yunoki, and E. Dagotto, Science **283**, 2034 (1999).
[3] T. Enoki and A. Miyazaki, Chem. Rev. **104**, 5449 (2004); H. Kobayashi, H. Cui, and A. Kobayashi, *ibid.* **104**, 5265 (2004), and references therein.
[4] H. Kobayashi, A. Kobayashi, and T. Cassoux, Chem. Soc. Rev. **29**, 325 (2000).
[5] S. Noguchi, A. Matsumoto, T. Matsumoto, T. Sugimoto, and T. Ishida, Physica B **346-347**, 397 (2004).
[6] S. Uji, H. Shinagawa, C. Terakura, T. Terashima, T. Yakabe, Y. Terai, M. Tokumoto, A. Kobayashi, H. Tanaka, and H. Kobayashi, Nature (London) **410**, 908 (2001).
[7] K. Kubo and N. Ohata, J. Phys. Soc. Jpn. **33**, 21 (1972).
[8] C. Hotta, M. Ogata, and H. Fukuyama, Phys. Rev. Lett. **95**, 216402 (2005).
[9] N. Hanasaki, H. Tajima, M. Matsuda, T. Naito, and T. Inabe, Phys. Rev. B **62**, 5839 (2000).
[10] T. Inabe and H. Tajima, Chem. Rev. **104**, 5503 (2004), and references therein.

[11] N. Hanasaki, M. Matsuda, H. Tajima, T. Naito, and T. Inabe, J. Phys. Soc. Jpn. **72**, 3226 (2003).
[12] F. Mila and X. Zotos, Europhys. Lett. **24**, 133 (1993).
[13] K. Sano and Y. Ono, J. Phys. Soc. Jpn. **63**, 1250 (1994).
[14] H. Yoshioka, M. Tsuchiizu, and Y. Suzumura, J. Phys. Soc. Jpn. **69**, 651 (2000).
[15] S. R. White, Phys. Rev. Lett. **69**, 2863 (1992).
[16] N. Shibata and C. Hotta (unpublished).
[17] H. Tsunetsugu, M. Sigrist, and K. Ueda, Phys. Rev. B **47**, 8345 (1993).
[18] Y. Otsuka, H. Seo, and Y. Motome, Physica B (to be published).
[19] D. J. García, K. Hallberg, C. D. Batista, M. Avignon, and B. Alascio, Phys. Rev. Lett. **85**, 3720 (2000).
[20] H. Tajima, G. Yoshida, M. Matsuda, K. Nara, K. Kajita, Y. Nishio, N. Hanasaki, T. Naito, and T. Inabe, Phys. Rev. B **78**, 064424 (2008).
[21] N. Hanasaki, K. Masuda, K. Kodama, M. Matsuda, H. Tajima, J. Yamaura, M. Takigawa, E. Ohmichi, T. Osada, T. Naito, and T. Inabe, J. Phys. Soc. Jpn. **75**, 104713 (2006).
[22] N. Hanasaki, K. Masuda, K. Kodama, M. Matsuda, H. Tajima, E. Ohmichi, T. Osada, T. Naito, and T. Inabe, J. Phys. Soc. Jpn. **75**, 033703 (2006).
[23] N. Hanasaki (private communication).